Day-Night and Energy Variations for Maximal Neutrino Mixing Angles

by

Mario Serna

Submitted to the Department of Physics
in partial fulfillment of the requirements for the degree of

Master of Science in Physics

at the

MASSACHUSETTS INSTITUTE OF TECHNOLOGY

June 1999

Author .....
Department of Physics
May 7, 1999

Certified by .....
Lisa Randall
Professor
Thesis Supervisor

Accepted by .....
Thomas J. Greytak
Professor, Associate Department Head for Education

Day-Night and Energy Variations for Maximal Neutrino Mixing Angles

by

Mario Serna

Submitted to the Department of Physics
on May 7, 1999, in partial fulfillment of the
requirements for the degree of
Master of Science in Physics

Abstract

It has been stated in the literature that the case of maximal mixing angle for ν_e leads to no day-night effect for solar neutrinos and an energy independent flux suppression of $\frac{1}{2}$. While the case of maximal mixing angle and Δm^2 in the MSW range of parameter space does lead to suppression of the electron neutrinos reaching the earth from the sun by $P_S = \frac{1}{2}$, the situation is different for neutrinos that have passed through the earth. We make the point that at maximal mixing, just as with smaller mixing angles, the earth regenerates the $|\nu_1\rangle$ state from the predominantly $|\nu_2\rangle$ state reaching the earth, leading to coherent interference effects. This regeneration can lead to a day-night effect and an energy dependence of the suppression of solar electron neutrinos, even for the case of maximal mixing. For large mixing angles, the energy dependence of the day-night asymmetry depends heavily on Δm^2. With a sufficiently sensitive measurement of the day-night effect, this energy dependence could be used to distinguish among the large mixing angle solutions of the solar neutrino problem.

Thesis Supervisor: Lisa Randall
Title: Professor of Physics

Acknowledgments

We would like to thank Paul Schechter for a useful conversation. We also greatly appreciate Kristin Burgess, Yang Hui He, and Jun Song for reviewing the manuscript. MS would like to thank the National Science Foundation (NSF) for her gracious fellowship, and the Air Force Institute of Technology (AFIT) for supporting this research. MS would like to thank Dr. Krastev for helping us understand the parameters involved in calculating the contour plots for the day-night effect. We would also like to thank Robert Foot for useful comments on the manuscript. This work is supported in part by funds provided by the U.S. Department of Energy (D.O.E.) under cooperative research agreement #DF-FC02-94ER40818.

Contents

1 Introduction **8**

2 Review of the Solar Neutrino Problem **11**

2.1 Overview 11

2.2 The nuclear reactions in the sun 11

2.3 The solar neutrino experiments 13

2.4 The missing neutrino flux 14

3 The MSW Effect **17**

3.1 Overview of the MSW solution to the solar neutrino problem 17

3.2 Derivation of MSW equations 18

3.3 Validity of the steady state approximation 26

4 The Day-Night Effect at Maximal Mixing **30**

4.1 Overview 30

4.2 Derivation of Equation (1.1) 31

4.3 Analysis at maximal mixing 33

4.4 Induced energy dependence 35

5 Conclusions **38**

A Calculation Methodology for the Day-Night Effect **39**

B The Zenith Distribution Function **43**

List of Figures

2-1 The solar neutrino energy spectrum, and the experiments sensitive to each reaction. [From Bahcall et. al. in Refs. [6, 8]] 14

2-2 The solar neutrino flux deficit for each of the three types of experiments. The hashed regions indicate the uncertainty in the theoretical estimate or the uncertainty in the measurement. [From Bahcall, Refs. [6, 5]] 15

3-1 MSW Solutions: The shaded areas are regions of the $\sin^2 2\theta_V$ - Δm^2 parameter space that are not excluded (i.e. allowed) by the measured neutrino flux rates of the chlorine, gallium, and water experiments at the 99% confidence level. [From Bahcall, Krastev, and Smirnov in Ref. [12]] 25

3-2 The regions satisfying the conditions for steady state density matrix. Above the line (a) is in steady state because of wave packet separation. Above the line (b) can be treated as steady state because of the eccentricity of the earth's orbit. Above the diagonal line (c) is in steady state because the region producing the neutrinos is much larger than an oscillation length, and this phase averaging survives until the neutrinos reach the vacuum. Above line (d) is in steady steady state because of the energy resolution of our detectors. 29

4-1 The evolution of $P_{\nu_e \to \nu_e}$ as the ensemble of neutrinos propagates across the center of the earth. The neutrinos enter the earth as an incoherent mixture of the energy eigenstates ν_1 and ν_2 which is almost completely ν_2. This plot shown is for $\Delta m^2 = 1.3 \times 10^{-5}$ eV^2 and a neutrino energy $E = 6.5$ MeV. 33

4-2 The day-night asymmetry ($A_{d-n} = (N - D)/(N + D)$) as a function of mixing parameters calculated using the density matrix. On the left is a three dimensional surface where the height of the surface is the day-night asymmetry. Notice that the exposed edge is calculated at maximal mixing and is clearly non-zero. On the right is a contour plot showing the lines of constant day-night asymmetry. 34

4-3 The predicted flux suppression as a function of energy. Notice that the predicted overall flux suppression is not 1/2, due to day-night effects, even though the mixing angle is maximal. The plot is for $\Delta m^2 = 1.0 \times 10^{-5}$ eV^2 which is near the border of the region excluded by the small day-night effect (A_{d-n}) measured at Super-Kamiokande. 36

4-4 The day-night asymmetry ($A_{d-n} = (N - D)/(N + D)$) as a function of recoil electron energy at Super-Kamiokande. Both plots are at maximal mixing angle, with Δm^2 at the upper and lower borders of the region disfavored by the smallness of the day-night effect observed at Super-Kamiokande. The rising line is for $\Delta m^2 = 2 \times 10^{-5}$ eV^2, and the descending line is for $\Delta m^2 = 3 \times 10^{-7}$ eV^2. 37

A-1 The Preliminary Reference Earth Model (PREM) electron density (N_e) profile of the earth. N_e is shown in units of Avogadro's number of electrons per cm^3. 40

B-1 The zenith distribution function at Super-Kamiokande. 44

List of Tables

2.1 The pp chain of nuclear reactions in the sun, and the energy of the resulting neutrinos. 12

Chapter 1

Introduction

The solar neutrino problem is the discrepancy between the theoretical estimates and the experimental measurements of the solar neutrino flux. This problem has been well established over the past thirty years with three separate types of experiments. Neutrino oscillations are thought to be a possible resolution to the discrepancy. Through most of the past thirty years theorists have assumed that the neutrino mixing must be small in analogy to the small mixing in the quark sector. The recent Super-Kamiokande announcement that atmospheric neutrinos are nearly maximally mixed has renewed much interest in the possibility that solar neutrinos might also be maximally mixed. In this document we will consider only two-neutrino mixings, so by "maximal mixing" we are referring to the possibility that the two lightest mass eigenstates, $|\nu_1\rangle$ and $|\nu_2\rangle$, with eigenvalues m_1 and m_2 respectively ($m_1 < m_2$), are each equal-probability superpositions of the flavor eigenstate $|\nu_e\rangle$ (electron neutrino) and some other state $|\nu_x\rangle$, where $|\nu_x\rangle$ can be any linear combination of $|\nu_\mu\rangle$ (muon neutrino) and $|\nu_\tau\rangle$ (tau neutrino). Many theoretical models have been proposed to predict the possibility of such maximal mixing (for example, see [27, 19, 18, 42, 28, 22, 33]). In this document we are concerned only with the MSW solutions to the solar neutrino problem, first proposed by Mikheyev, Smirnov, and Wolfenstein [48, 39, 40], while the alternative possibility of nearly maximally mixed vacuum oscillations has been considered by other authors [20]. The MSW effect results from the neutrino interaction with matter, causing an enhancement of the conversion process transforming

ν_e into ν_x. The MSW effect is also capable of driving neutrinos back towards a ν_e state after passing through the earth. This process would result in a change in the ν_e flux between daytime and nighttime measurements, a phenomenon known as the day-night effect, or more generally zenith angle dependence. Over the past decade there have been extensive studies of the day-night effect [21, 16, 17, 36, 37, 38, 10, 49] which have been mostly concerned with the small mixing angle solutions to the solar neutrino problem. Most of these studies have used the Mikheyev-Smirnov expression [41] to describe the effect of the earth on the solar neutrinos, which we will hereafter refer to as Eq. (1.1):

$$P_{SE} = \frac{P_S - \sin^2\theta_V + P_{2e}(1 - 2P_S)}{\cos 2\theta_V} \ . \tag{1.1}$$

Here P_{SE} is the probability that an electron neutrino originating in the sun will be measured as an electron neutrino after passing through the earth, P_S is the probability that an electron neutrino ($|\nu_e\rangle$) originating in the sun will be measured as an electron neutrino upon reaching the earth, P_{2e} is the probability that a pure $|\nu_2\rangle$ eigenstate entering the earth will be measured as an electron neutrino when it emerges, and θ_V is the vacuum mixing angle, defined through

$$|\nu_1\rangle = |\nu_e\rangle \cos\theta_V - |\nu_x\rangle \sin\theta_V \ , \tag{1.2a}$$

$$|\nu_2\rangle = |\nu_x\rangle \cos\theta_V + |\nu_e\rangle \sin\theta_V \ . \tag{1.2b}$$

In the previous studies of the day-night effect several authors have claimed that there is no day-night effect at $P_S = \frac{1}{2}$ (for example, [10, 17]). We wish to emphasize, however, that the case of maximal mixing is an exception to this statement. For maximal mixing Eq. (1.1) is ill-defined, since $\cos 2\theta_V = 0$, and we will show below that generically there *is* a day-night effect for this case. Nonetheless, we have no disagreements with either the equations or the contour plots in the aforementioned

papers, which in fact do show non-zero day-night effects at maximal mixing. The purpose of this thesis is to clarify the previous papers, and also to investigate more carefully the role of the day-night effect for maximal mixing. We will show that at maximal mixing $P_{SE} \neq \frac{1}{2}$, implying a day-night effect and an often overlooked energy-dependence of the suppression of the solar neutrino flux.

In the remainder of this document we explain in more detail why maximal mixing can result in a day-night effect. In Chapter 2 we begin with the background of the solar neutrino problem. Chapter 3 then explains the MSW solution to the solar neutrino problem. Next, in Chapter 4, we review the derivation of Eq. (1.1) as given by Mikheyev and Smirnov [41], we resolve the maximal mixing ambiguity, and we present results of numerical calculations showing the day-night effect at maximal mixing. Finally Chapter 5 summarizes the results of the thesis. In the appendices, we provide greater details concerning the numerical calculations presented in Chapter 4.

Chapter 2

Review of the Solar Neutrino Problem

2.1 Overview

The solar neutrino problem is the discrepancy between the experimental measurements and the theoretical predictions of the neutrino flux from the sun. The theoretical predictions come from models of stellar interiors that calculate the neutrinos generated in nuclear reactions. These models are well-believed and have stood up to robust tests in other contexts. However, direct experimental measurement consistently yields a solar neutrino flux significantly below the theoretical prediction. In this chapter we review the major components of the solar neutrino problem: the nuclear reactions involved, the solar neutrino detectors, and the consequences of the missing neutrino flux.

2.2 The nuclear reactions in the sun

Solar neutrinos provide a unique opportunity to see the nuclear reactions in the core of the sun [9]. Because of the high opacity of the solar interior, the photons generated in these regions are heavily scattered and most of the information about the processes which created them has been lost [3]. Neutrinos, however, can relay this information

Reaction	Abbreviation	Neutrino Energy (MeV)
$p + p \rightarrow {}^2H + e^+ + \nu_e$	pp	$0.0 - 0.4$
$p + e^- + p \rightarrow {}^2H + \nu_e$	pep	1.4
${}^2H + p \rightarrow {}^3He + \gamma$		
${}^3He + {}^3He \rightarrow {}^4He + 2p$		
${}^3He + {}^4He \rightarrow {}^7Be + \gamma$		
$e^- + {}^7Be \rightarrow {}^7Li + \nu_e$	^{7}Be	0.38, 0.86
${}^7Li + p \rightarrow {}^4He + {}^4He$		
${}^7Be + p \rightarrow {}^8B + \gamma$		
${}^8B \rightarrow {}^8Be + e^+ + \nu_e$	^{8}B	$0.0 - 14$
${}^3He + p \rightarrow {}^4He + e^+ + \nu_e$	hep	$1 - 18.8$

Table 2.1: The pp chain of nuclear reactions in the sun, and the energy of the resulting neutrinos.

since they have an extraordinarily small cross section which allows them to leave the sun almost unaffected. Through models of the solar interior we can predict the quantity and the energy of the neutrinos produced in the sun. These models entail complicated numerical simulations that establish hydrostatic equilibrium between the gravitational force and the thermal pressure from the nuclear reactions, while accounting for opacity, heat transfer, abundance and diffusion of elements. Each of these factors feed back into calculating the rates of all the nuclear reactions which in turn affects the thermal pressure, opacity, and abundances of the elements. The computer code is iterated until a steady state solution is attained. Similar models are used to simulate the complete life of the star. There are two main sequences of nuclear reactions occurring in the solar interior: the pp chain and the CNO chain. The pp (proton - proton) chain dominates the energy production in the sun, while the CNO (carbon - nitrogen - oxygen) chain accounts for only 1% of the total power output of the sun [26]. Table 2.2 shows nuclear reactions in the pp chain and the expected energy range of the neutrinos in these reactions [5, 13]. Fig. 2-1, in the next section, also shows the neutrino energy spectrum from each of these reactions. Measurement of a neutrino flux from these reactions consistent with theoretical prediction would be very strong evidence that our understanding of the physics of the solar interior is correct.

2.3 The solar neutrino experiments

Experiments have been designed and built to measure the solar neutrino flux [3]. There are currently three main types of experiments; they function by detecting the neutrino reactions in chlorine, gallium, and water. The chlorine experiment (Homestake[23]) relies on the reaction

$$^{37}\mathrm{Cl} + \nu_{\mathrm{e}} \rightarrow \mathrm{e}^{-} + ^{37}\mathrm{Ar} \tag{2.1}$$

to convert chlorine into argon and is sensitive to neutrino energies greater than 0.9 MeV. The experiment utilizes the fact that argon is a noble gas and can be separated from the other reactants. The quantity of the isotope ^{37}Ar is measured by monitoring its decay. The gallium experiments (GALLEX[29] and SAGE[31]) rely on the reaction

$$^{71}\mathrm{Ga} + \nu_{\mathrm{e}} \rightarrow \mathrm{e}^{-} + ^{71}\mathrm{Ge} \tag{2.2}$$

to convert gallium into germanium and are sensitive to neutrino energies above 0.2 MeV [7]. Again, one performs the measurement by counting the amount of germanium produced after exposing the gallium target to solar neutrinos. The chlorine and the gallium experiments both operate by separating and measuring the products of the reactions after weeks of exposure to solar neutrinos. In contrast, the water experiments (Kamiokande[32] and Super-Kamiokande[49]) measure the Cerenkov radiation from the recoil electrons in the scattering reaction

$$\nu_e + \mathrm{e}^{-} \rightarrow \nu_{\mathrm{e}} + \mathrm{e}^{-}. \tag{2.3}$$

The Cerenkov radiation allows both the energy of the electron and direction of the momentum of the electron to be measured in real time. The energy and momentum vector of the recoil electron in turn provide indirect information about the energy and momentum vector of the incoming neutrino. The water experiments are sensitive to neutrino energies greater than 6.5 MeV. The predicted neutrino energy spectrum and

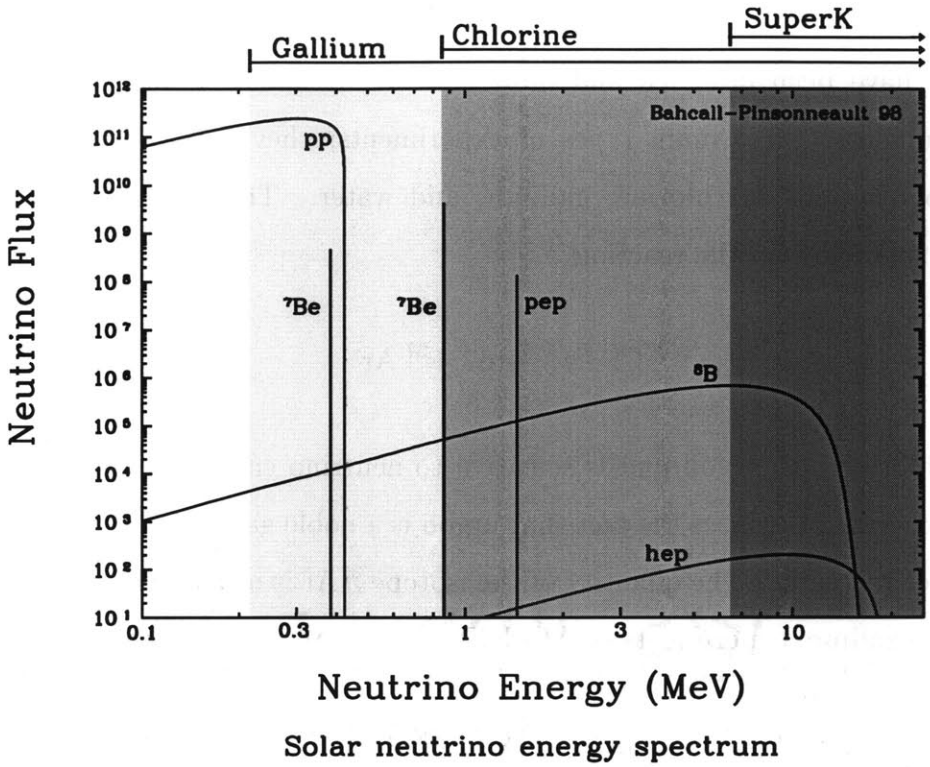

Figure 2-1: The solar neutrino energy spectrum, and the experiments sensitive to each reaction. [From Bahcall et. al. in Refs. [6, 8]]

the experiments sensitive to the various energy ranges can be seen in Fig. 2-1. These three types of solar neutrino experiments, involving chlorine, gallium, and water, have collected over thirty years of data spanning most of the neutrino energy spectrum.

2.4 The missing neutrino flux

The disagreement between the predicted neutrino flux from the solar models and the measured neutrino flux from the chlorine, gallium, and water neutrino detectors is called the solar neutrino problem. The chlorine experiment measures only 1/3 the theoretically predicted flux, the water experiments only 1/2, and the gallium experiments only 3/5. Fig. 2-2 shows the comparison between the experimental measurements and theoretical predictions. The hashed regions indicate the uncertainty in the theoretical estimate or the uncertainty in the measurement. This disagreement is

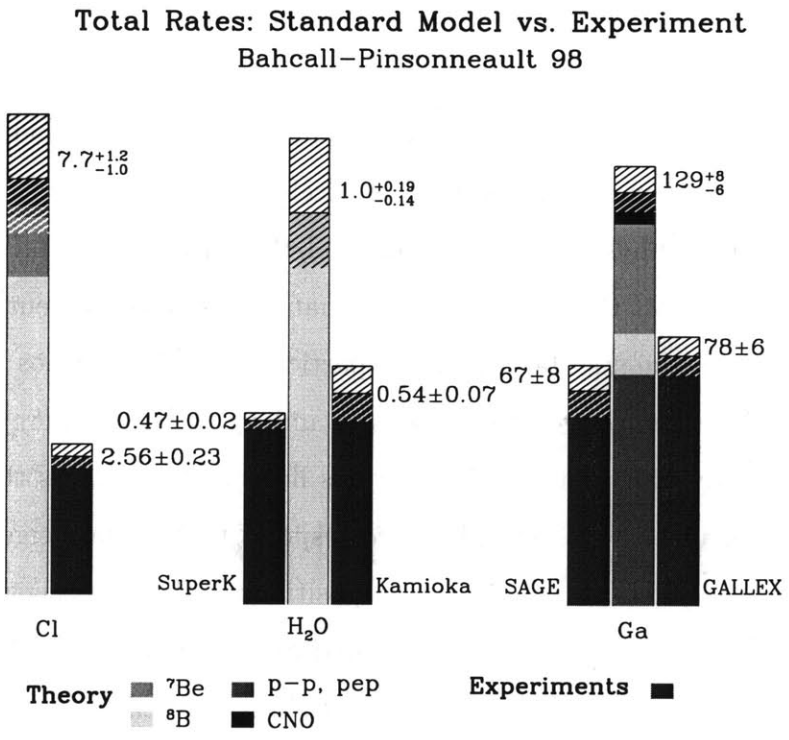

Figure 2-2: The solar neutrino flux deficit for each of the three types of experiments. The hashed regions indicate the uncertainty in the theoretical estimate or the uncertainty in the measurement. [From Bahcall, Refs. [6, 5]]

the solar neutrino problem; more than thirty years of measurements by three different types of experiments and continual refinement of the solar model with improved cross sections and accounting for smaller order effects have not resolved the disparity.

The disagreement between theory and experiment must mean one of three things: the solar model is incomplete, our understanding of the neutrino cross section is flawed, or something beyond the standard model of particle physics happens to the neutrinos in transit to the earth. Currently, measurements of the speed of sound in the sun (known as helioseismology) lead us to have great faith in the standard solar model [8]. Additionally, variants of the standard solar model also have large disagreements with the measured neutrino flux making it hard to believe that the solar model is the problem. A wide variety of accelerator experiments verify our understanding of particle physics cross sections and the nuclear reactions. Therefore, physicists strongly suspect the mystery lies in what happens to the neutrinos as they travel to the earth. In the standard model of particle physics neutrinos are massless. This means that the flavor eigenstates (ν_e, ν_μ, and ν_τ) and the energy eigenstates can be simultaneously diagonlaized. If neutrinos have non-zero mass then it is possible that the flavor eigenstates would not correspond to the mass eigenstates, and therefore the flavor eigenstates could be superpositions of the mass eigenstates. This superposition of mass eigenstates results in neutrino oscillations. Quantum mechanical interference between mass eigenstates oscillating at different frequencies causes a component of the electron neutrino to oscillate into a neutrino of a different flavor. Because the solar neutrino experiments are mostly sensitive to ν_e measurements, if the neutrinos oscillate into a different flavor then they would pass through the experiments undetected. If the lepton mixing mirrors the quark mixing, then one would expect the neutrinos to be only slightly mixed. However, a small mixing leads to only a small fraction of ν_e oscillating into some other flavor ν_x, and this would not account for the large discrepancy between experiment and theory. Nonetheless, the neutrino oscillation hypothesis is the dominant candidate proposed to solve the solar neutrino problem.

Chapter 3

The MSW Effect

3.1 Overview of the MSW solution to the solar neutrino problem

The MSW effect, first proposed by Mikheyev, Smirnov, and Wolfenstein [48, 39, 40], allows a small mixing angle to significantly change the fraction of neutrinos arriving at the earth. The effect results from the neutrino interaction with matter which shifts the instantaneous energy eigenvalues of the Hamiltonian. In this high density medium of the solar interior the $|\nu_e\rangle$ state,

$$|\nu_e\rangle = \cos\theta_M|\nu_1\rangle + \sin\theta_M|\nu_2\rangle, \tag{3.1}$$

is a superposition of the two instantaneous mass eigenstates with a definite phase relationship expressed in terms of the matter mixing angle θ_M. If the states evolve adiabatically, the fraction of the neutrinos in each adiabatic states, $|\nu_1\rangle$ and $|\nu_2\rangle$, remains approximately constant. However, in the vacuum the $|\nu_e\rangle$ state is given by a different superposition,

$$|\nu_e\rangle = \cos\theta_V|\nu_1\rangle + \sin\theta_V|\nu_2\rangle, \tag{3.2}$$

expressed in terms of the vacuum mixing angle θ_V which is significantly different from the high density matter mixing angle θ_M. The change in the definition of the $|\nu_e\rangle$ state

in the vacuum compared to the high density region is responsible for the conversion process transforming ν_e into ν_x, where ν_x is some neutrino flavor other than ν_e. This conversion is a possible solution to the solar neutrino problem by enabling some of the ν_e generated in the sun to be converted into a flavor that is not detected by the neutrino experiments, even with a small vacuum mixing angle.

In this document we are concerned only with the MSW solutions to the solar neutrino problem. The alternative possibility of nearly maximally mixed vacuum oscillations has been considered by other authors [20].

3.2 Derivation of MSW equations

We now present a more detailed derivation of the MSW effect. First we derive the MSW equations of motion for an individual neutrino. We then find the energy eigenstates of the system and use them to find the wave function amplitudes for electron neutrinos produced in the sun and evolved into the vacuum. To describe the ensemble of neutrinos we introduce the density matrix. After averaging out the rapid oscillations we find a steady state solution to the density matrix equations of motion. We average this solution over the regions of neutrino production.

We begin by finding the MSW equations of motion for an individual neutrino. The coupling describing the interaction between electron neutrinos and electrons is

$$H_{int} = \sqrt{2} G_F N_e, \tag{3.3}$$

where N_e is the number density of electrons. This contribution to the interaction Hamiltonian is added to the Schrödinger equation written in the flavor basis. We assume that $|\nu_e\rangle$ can be written as a superposition of only two mass eigenstates, $|\nu_1\rangle$ and $|\nu_2\rangle$. We let $|\nu_x\rangle$ denote the orthogonal linear combination of $|\nu_1\rangle$ and $|\nu_2\rangle$, which might be any superposition of $|\nu_\mu\rangle$ (muon neutrino) and $|\nu_\tau\rangle$ (tau neutrino). The

transformation between the ν_1-ν_2 and ν_e-ν_x bases is then given by

$$\begin{pmatrix} C_{\nu_1} \\ C_{\nu_2} \end{pmatrix} = \begin{pmatrix} \cos\theta_V & -\sin\theta_V \\ \sin\theta_V & \cos\theta_V \end{pmatrix} \begin{pmatrix} C_{\nu_e} \\ C_{\nu_x} \end{pmatrix} , \tag{3.4}$$

where the variable θ_V is the vacuum mixing angle, and $C_\nu \equiv \langle \nu | \Psi \rangle$ for $\nu = \nu_1$, ν_2, ν_e or ν_x. This equation can be written compactly by introducing the index notation

$$C_{\nu_i} = U^\dagger_{if} C_{\nu_f} , \tag{3.5}$$

where the repeated index f is summed over ν_e and ν_x, and i is summed over the mass eigenstates. The Schrödinger equation for this system is:

$$i\partial_t \begin{pmatrix} C_{\nu_e} \\ C_{\nu_x} \end{pmatrix} = \left[U \begin{pmatrix} p + \frac{m_1^2}{2p} & 0 \\ 0 & p + \frac{m_2^2}{2p} \end{pmatrix} U^\dagger + \begin{pmatrix} \sqrt{2} G_F N_e & 0 \\ 0 & 0 \end{pmatrix} \right] \begin{pmatrix} C_{\nu_e} \\ C_{\nu_x} \end{pmatrix} , \tag{3.6}$$

where we have expanded the energy in the ultra-relativistic limit so that $E = p + \frac{m^2}{2p}$. We now substitute U into the Schrödinger equation, obtaining

$$i\partial_t \begin{pmatrix} C_{\nu_e} \\ C_{\nu_x} \end{pmatrix} = \begin{pmatrix} B & A \\ A & -B \end{pmatrix} \begin{pmatrix} C_{\nu_e} \\ C_{\nu_x} \end{pmatrix} \tag{3.7}$$

where

$$\Delta_0 \equiv \frac{1}{2p}(m_2^2 - m_1^2) \tag{3.8}$$

$$A \equiv \frac{\Delta_0}{2} \sin 2\theta_V \tag{3.9}$$

$$B \equiv \frac{\sqrt{2}}{2} G_F N_e - \frac{\Delta_0}{2} \cos 2\theta_V , \tag{3.10}$$

and where we have dropped the term $p + \frac{(m_1^2 + m_2^2)}{4p} + \frac{\sqrt{2}}{2} G_F N_e$ which is proportional to the identity, because terms proportional to the identity cannot contribute to mixing.

The eigenvalues are $\pm\lambda(N_e)$, where $\lambda(N_e) = \sqrt{A^2 + B^2}$, and the eigenvectors are:

$$v_- = \begin{pmatrix} \sqrt{\frac{\lambda - B}{2\lambda}} \\ -\sqrt{\frac{\lambda + B}{2\lambda}} \end{pmatrix} \text{ , and } v_+ = \begin{pmatrix} \sqrt{\frac{\lambda + B}{2\lambda}} \\ \sqrt{\frac{\lambda - B}{2\lambda}} \end{pmatrix}. \tag{3.11}$$

Since these eigenvectors form the matrix that will diagonalize the interaction matrix in the presence of matter, it is useful to parameterize them by a matter mixing angle $\theta_M(N_e)$:

$$\cos\theta_M = \sqrt{\frac{\lambda - B}{2\lambda}}, \quad \text{and} \quad \sin\theta_M = \sqrt{\frac{\lambda + B}{2\lambda}}, \tag{3.12}$$

or equivalently

$$\lambda \cos 2\theta_M = -B, \tag{3.13}$$

or

$$\lambda \sin 2\theta_M = A. \tag{3.14}$$

Defining the matrix

$$U(\theta_M) = \begin{pmatrix} \cos\theta_M & \sin\theta_M \\ -\sin\theta_M & \cos\theta_M \end{pmatrix}, \tag{3.15}$$

the Hamiltonian can be diagonalized as

$$U(\theta_M) \begin{pmatrix} -\lambda & 0 \\ 0 & \lambda \end{pmatrix} U^\dagger(\theta_M) = \begin{pmatrix} B & A \\ A & -B \end{pmatrix}. \tag{3.16}$$

We maintain the notation introduced in Eq. (3.5) so that $C_{\nu_i}(\theta_M) = U^\dagger_{if}(\theta_M) C_{\nu_f}$ in or out of matter, where $C_{\nu_i}(\theta_M) \equiv \langle \nu_i | \Psi \rangle$ denotes the amplitude for the overlap of the neutrino state with instantaneous mass eigenstates $|\nu_i\rangle$.

To describe the evolution of the neutrinos as they travel to the earth from their creation point in the sun, it is useful to develop the adiabatic approximation, in which one assumes that the density changes imperceptibly within an oscillation length. Remembering that U, θ_M, and λ are all functions of the local electron density N_e, and hence functions of time, we write the Schrödinger equation in the basis $\nu_i(\theta_M)$ of

the instantaneous mass eigenstates:

$$i\partial_t \begin{pmatrix} C_{\nu_1} \\ C_{\nu_2} \end{pmatrix} = \begin{pmatrix} -\lambda & 0 \\ 0 & \lambda \end{pmatrix} \begin{pmatrix} C_{\nu_1} \\ C_{\nu_2} \end{pmatrix} + (i\partial_t U^\dagger) U \begin{pmatrix} C_{\nu_1} \\ C_{\nu_2} \end{pmatrix} \tag{3.17}$$

$$= \begin{pmatrix} -\lambda & 0 \\ 0 & \lambda \end{pmatrix} \begin{pmatrix} C_{\nu_1} \\ C_{\nu_2} \end{pmatrix} + i \begin{pmatrix} 0 & -\partial_t \theta_M \\ \partial_t \theta_M & 0 \end{pmatrix} \begin{pmatrix} C_{\nu_1} \\ C_{\nu_2} \end{pmatrix} . \tag{3.18}$$

The adiabatic approximation is the assumption that the off-diagonal terms $\partial_x \theta_M$ can be neglected, in which case the equation is easily integrated:

$$\begin{pmatrix} C_{\nu_1}(t_f) \\ C_{\nu_2}(t_f) \end{pmatrix} \approx \begin{pmatrix} e^{+i\phi(t_f)} & 0 \\ 0 & e^{-i\phi(t_f)} \end{pmatrix} \begin{pmatrix} C_{\nu_1}(t_0) \\ C_{\nu_2}(t_0) \end{pmatrix} , \tag{3.19}$$

where

$$\phi(t_f) = \int_{t_0}^{t_f} \lambda(t) dt . \tag{3.20}$$

Because the adiabatic states form a complete basis, we can always write the exact solution as a superposition of the two adiabatic states. This final superposition is expressed by two unknown variables, a_1 and a_2 where $|a_1|^2 + |a_2|^2 = 1$. The $|a_2|^2$ parameter represents the probability of a non-adiabatic transition, which is most likely to happen when the neutrinos cross resonance, the density at which $B = 0$, when the two eigenvalues become nearly equal. Likewise $|a_1|^2 = 1$ would represent adiabatic evolution. Given any initial state $\nu_f(t_0)$ in the flavor basis, the final state can be written in the general form:

$$\begin{pmatrix} C_{\nu_1}(t_f) \\ C_{\nu_2}(t_f) \end{pmatrix} = \begin{pmatrix} a_1 & a_2 \\ -a_2^* & a_1^* \end{pmatrix} \begin{pmatrix} e^{+i\phi(t_f)} & 0 \\ 0 & e^{-i\phi(t_f)} \end{pmatrix} U^\dagger\big(\theta_M(t_0)\big)\ \nu_f(t_0) . \tag{3.21}$$

For an electron neutrino originating in a medium of mixing angle θ_M, the above equation implies that the final state in the vacuum is given by

$$\begin{pmatrix} C_{\nu_1}(t_f) \\ C_{\nu_2}(t_f) \end{pmatrix} \equiv \begin{pmatrix} A_1 \\ A_2 \end{pmatrix} = \begin{pmatrix} a_1 \cos\theta_M e^{+i\phi} + a_2 \sin\theta_M e^{-i\phi} \\ -a_2^* \cos\theta_M e^{+i\phi} + a_1^* \sin\theta_M e^{-i\phi} \end{pmatrix} . \tag{3.22}$$

We now go on to talk about the ensemble of neutrinos reaching the earth. To

describe a quantum mechanical ensemble of neutrinos, it is useful to introduce the density matrix

$$\rho \equiv \sum_i f_i |\nu_i\rangle\langle\nu_i| \ , \tag{3.23}$$

where f_i denotes the probability that the particle is in the quantum state $|\nu_i\rangle$. The density matrix corresponding to a single neutrino as described by Eq. (3.22) is therefore given by

$$\rho = \begin{pmatrix} |A_1|^2 & A_1 A_2^* \\ A_1^* A_2 & |A_2|^2 \end{pmatrix} \ , \tag{3.24}$$

where

$$|A_1|^2 = \frac{1}{2}\left[1 + \cos 2\theta_M \left(1 - 2|a_2|^2\right)\right] + \frac{1}{2}\left[a_1 a_2^* \sin 2\theta_M e^{2i\phi(t_f)} + c.c\right] \tag{3.25}$$

$$A_1 A_2^* = \frac{1}{2}\sin 2\theta_M \left[a_1^2 e^{2i\phi(t_f)} - a_2^2 e^{-2i\phi(t_f)}\right] - a_1 a_2 \cos 2\theta_M \tag{3.26}$$

$$|A_2|^2 = \frac{1}{2}\left[1 - \cos 2\theta_M \left(1 - 2|a_2|^2\right)\right] - \frac{1}{2}\left[a_1 a_2^* \sin 2\theta_M e^{2i\phi(t_f)} + c.c\right] \tag{3.27}$$

In Sec. 3.3 we explain why this process allows us to eliminate the terms that have rapidly oscillating phases. In particular, the phase angle $\phi(t_f)$ and the phases of the complex numbers a_1 and a_2 are all rapidly varying functions of the neutrino energy, the location in the sun where the neutrino is produced, and the precise time of day and year at which the neutrino is observed. The density matrix which describes the ensemble of observed neutrinos is constructed by averaging over these quantities, so any quantity with a rapidly oscillating phase will average to zero. This is equivalent to the statement that the ν_1 and ν_2 components arriving at the earth are incoherent, so we average over their phases. The matrix elements of the phase-averaged density matrix are given by

$$\langle|A_1|^2\rangle = \frac{1}{2}\left[1 + \cos 2\theta_M \left(1 - 2|a_2|^2\right)\right] \tag{3.28}$$

$$\langle A_1 A_2^*\rangle = 0 \tag{3.29}$$

$$\langle|A_2|^2\rangle = \frac{1}{2}\left[1 - \cos 2\theta_M \left(1 - 2|a_2|^2\right)\right] \ . \tag{3.30}$$

The term $|a_2|^2 \equiv P_{\rm jump}$ is the probability of crossing from one adiabatic state to the other during the time evolution of these operators. An approximate expression for $P_{\rm jump}$ can be found by using a linear approximation for the density profile at resonance [43], yielding

$$P_{\rm jump} = \exp\left(-\frac{\pi\Delta m^2 \sin^2(2\theta_V) N(x_{\rm res})}{4p\cos(2\theta_V) N'(x_{\rm res})}\right) . \tag{3.31}$$

Here $N(x_{\rm res})$ is the density at the point where the neutrino crosses resonance, and $N'(x_{\rm res})$ is the first derivative of the density at resonance. More accurate approximations to $P_{\rm jump}$ and the details of their derivation can be found in Refs. [14, 15] and the references therein.

The density matrix corresponding the ensemble of observed neutrinos must be obtained by averaging over the production sites in the sun. While we have already made use of this fact in dropping all terms with rapidly oscillating phases, we must still average the slowly varying terms which remain. Letting ${}^8B(r)$ denote the normalized probability distribution for production at a distance r from the center of the sun, one finds

$$\rho = \begin{pmatrix} \frac{1}{2} + C_0 & 0 \\ 0 & \frac{1}{2} - C_0 \end{pmatrix} , \tag{3.32}$$

where

$$C_0 = \frac{1}{2}\int_0^{R_{\rm sun}} dr\ {}^8B(r)\ \cos\Big(2\theta_M(r)\Big)\ (1 - 2P_{\rm jump}) . \tag{3.33}$$

Note that the diagonal entries of ρ are just the fractions k_1 and k_2 of ν_1 and ν_2 flux from the sun. Therefore

$$k_1 = \frac{1}{2} + C_0\ ,\ k_2 = \frac{1}{2} - C_0\ . \tag{3.34}$$

Finally, we transform to the ν_e-ν_x basis, so

$$\rho^{\nu_e\nu_x} = U(\theta_V)\rho U^\dagger(\theta_V) \equiv \begin{pmatrix} \rho_{ee} & \rho_{ex} \\ \rho_{xe} & \rho_{xx} \end{pmatrix} . \tag{3.35}$$

One then finds that the probability of observing a neutrino reaching the surface of

the earth as an electron neutrino is given by

$$P_S = \rho_{ee} = \frac{1}{2} + C_0 \cos 2\theta_V \ . \tag{3.36}$$

The off-diagonal matrix element is given by

$$\rho_{xe} = -C_0 \sin 2\theta_V \ . \tag{3.37}$$

Our numerical simulations have all been performed by integrating Eq. (3.7) to solve for P_{2e}, and also by integrating the density matrix equations of motion. The evolution of the density matrix is given by

$$i\hbar\partial_t \rho = -[\rho, H]. \tag{3.38}$$

Using Eq. (3.38) with the Hamiltonian in the flavor basis, we find that our new equations of motion are

$$i\partial_t \rho_{ee} = A(\rho_{xe} - \rho^*_{xe}) \tag{3.39}$$

$$i\partial_t \rho_{xe} = 2(A\rho_{ee} - B\rho_{xe}) - A \ , \tag{3.40}$$

where A and B are defined in Eqs. (3.9) and (3.10). This allows us to perform calculations using the complete mixed ensemble. The expressions given in Eqs. (3.36) and (3.37) form a steady state solution of the density matrix equations of motion in the vacuum.

Applying the MSW effect to the neutrinos produced in the sun creates three possible solutions to the solar neutrino problem, pictured in Fig. 3-1. The plot is given as a function of the two basic parameters involved in neutrino oscillations: the vacuum mixing angle expressed as $\sin^2 2\theta_V$ and the mass squared difference between the two mass eigenstates Δm^2. The shaded areas are regions of the $\sin^2 2\theta_V$ - Δm^2 parameter space that are not excluded (i.e. allowed) by the measured neutrino flux rates of the chlorine, gallium, and water experiments at the 99% confidence level.

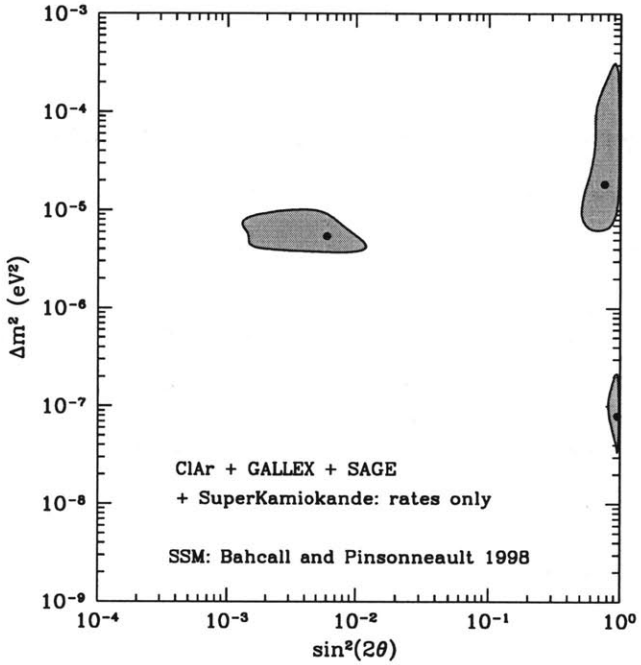

Figure 3-1: MSW Solutions: The shaded areas are regions of the $\sin^2 2\theta_V$ - Δm^2 parameter space that are not excluded (i.e. allowed) by the measured neutrino flux rates of the chlorine, gallium, and water experiments at the 99% confidence level. [From Bahcall, Krastev, and Smirnov in Ref. [12]]

3.3 Validity of the steady state approximation

Most of the work in the past decade on the MSW effect has assumed that the ensemble of neutrinos reach the earth in a steady state solution of the density matrix (i.e., in an incoherent mixture of the mass eigenstates ν_1 and ν_2). There are several reasons that the neutrinos reach the earth in a steady state: (a) The separation of the $|\nu_1\rangle$ and $|\nu_2\rangle$ wave-packets while propagating from the sun to the earth exceeds the size of the individual wave packets, eliminating the interference effects. (b) The eccentricity of the earth's orbit results in a daily change of the earth-sun radius larger than the vacuum oscillation length of the neutrinos. (c) The neutrinos are produced in a region much larger than their local oscillation length. (d) The energy resolution of the current detectors coupled with the earth-sun radius perform an average. We now proceed to map out the parameter space justifying where the steady state approximation is valid. First we consider the separation of the two eigenstates during transit to the earth. This results in system that is an incoherent superposition of $|\nu_1\rangle$ and $|\nu_2\rangle$. The width of the wave-packets, σ_x, is given by Ref. [34]:

$$\sigma_x \approx 0.9 \times 10^{-7} \text{ cm}. \tag{3.41}$$

This results in a coherence length given by:

$$L_{coh} = 2\sqrt{2}\sigma_x \frac{2E^2}{\Delta m^2}. \tag{3.42}$$

We lose coherence between the mass eigenstates if $L_{coh} < 1$ AU $= 1.5 \times 10^{13}$ cm. If we require that the incoherence condition apply up to 14 MeV to include all ^8B neutrinos, we find that for all of $\sin^2 2\theta_V$ where $\Delta m^2 > 6.63 \times 10^{-6}$ eV^2 the wave-packets have separated upon reaching earth. This corresponds to the region above the line labeled (a) in Fig. 3-2. Because there is a continuous beam of neutrinos arriving from the sun, we can ignore the fact that the lighter mass eigenstate arrives first, and simply drop terms that rapidly oscillate due to the lack of interference between the two states.

In the previous case the interference effects vanish because of a loss of coherence between the mass eigenstates for a neutrino produced at a specific place and time. In the remaining topics the interference effects vanish due to averaging over the ensemble of neutrinos which reach the detector.

Next, we analyze the effect of the eccentricity of the earth's orbit . We are interested in day-night effects; therefore, if the earth-sun radius changes by more than an oscillation length during one day, this will result in washing out any phase dependence in the results measured over a period of one year. Between perihelion and aphelion the earth-sun radius changes by $2e(1\text{ AU}) = 5.1 \times 10^{11}$ cm, where $e = 0.017$ is the earth eccentricity. The earth-sun radius changes by this quantity once every 180 days giving an average daily change in radius of 2.83×10^9cm. This ensures our incoherent phase for $\Delta m^2 > 1.2 \times 10^{-6}$ eV^2. This region is denoted by everything above the line marked (b) in Fig. 3-2.

Third, we study the impact of where the neutrinos were produced. If the neutrino region of production is greater than the local oscillation length of the neutrinos, then neutrinos of all possible phases exist in the ensemble. For a continuous beam of neutrinos, this also results in dropping the rapidly oscillating terms. The condition is satisfied for the entire parameter space under consideration $0.001 < \sin^2 2\theta_V < 1$ and 1×10^{-11} eV^2 $< \Delta m^2 < 1 \times 10^{-3}$ eV^2. However, one must be careful in making this statement. Although the region of production may be greater than the neutrino oscillation length in the sun, the neutrinos could undergo a non-adiabatic transition, and thus bring a specific phase into dominance. This is the case for vacuum oscillations ($\Delta m^2 \approx 4 \times 10^{-10}$ eV^2). The ^8B neutrinos are produced mostly at $R_{^8B} = 0.046\ R_{sun} = 3.2 \times 10^9$cm. The vacuum oscillation length is on the order of 1 AU. However the oscillations length near the solar core where these neutrinos are produced is about 1.8×10^7cm $\ll R_{^8B}$. Although the neutrinos are produced in a region larger than their oscillation length, they acquire roughly the same phase in the process of leaving the sun. This occurs because the density change upon leaving the sun occurs more rapidly than the oscillation length of the neutrinos, violating the condition of adiabaticity. To express this quantitatively we estimate that

if $P_{\text{jump}} < 0.1$ for 14 MeV neutrinos that the initial randomly distributed oscillation phases at the time of production will persist as the neutrinos leave the sun and enter the vacuum. This leads to a steady state solution applicable in the parameter space above the diagonal line labeled (c) shown in Fig. 3-2.

Last, we study the impact of the energy resolution on our ability to discriminate phases. Assuming perfect coherence between the two mass eigenstates the phase upon reaching the earth is given by

$$\phi = \frac{\Delta m^2 (1 \text{ AU})}{4p\hbar c}. \tag{3.43}$$

Our uncertainty in energy impacts our uncertainty in phase through error propagation:

$$\delta\phi = \left|\frac{d\phi}{dp}\right| \delta p = \frac{\Delta m^2 (1 \text{ AU})}{4p^2\hbar c}\delta p. \tag{3.44}$$

If the uncertainty in our phase is greater than 2π we are again justified in treating our ensemble as a steady state. Using conservative figures for energy ($p = 14$ MeV), and the energy resolution ($\delta p \approx 1$ MeV) [11], we find that for $\Delta m^2 > 6.5 \times 10^{-9}$ eV^2 we are justified in the steady state approximation. This inequality corresponds to parameter space above the line labeled (d) in Fig. 3-2. Recently Ref. [24] also reached the same conclusions outlined in this section.

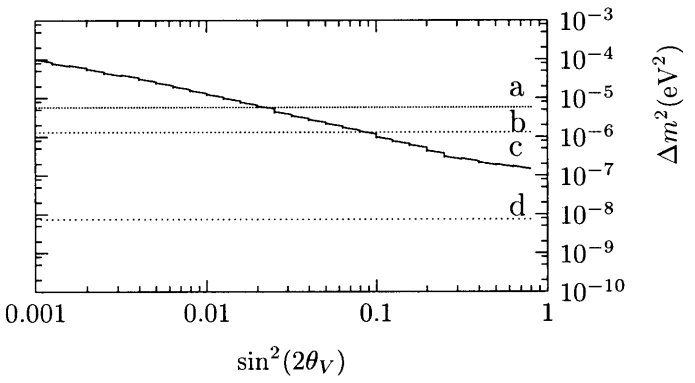

Figure 3-2: The regions satisfying the conditions for steady state density matrix. Above the line (a) is in steady state because of wave packet separation. Above the line (b) can be treated as steady state because of the eccentricity of the earth's orbit. Above the diagonal line (c) is in steady state because the region producing the neutrinos is much larger than an oscillation length, and this phase averaging survives until the neutrinos reach the vacuum. Above line (d) is in steady steady state because of the energy resolution of our detectors.

Chapter 4

The Day-Night Effect at Maximal Mixing

4.1 Overview

We have thus far explained the solar neutrino problem, and the MSW solution to the problem. The neutrino interaction with matter can also play a role when the neutrinos pass through the earth. This process would result in a change in the ν_e flux between daytime and nighttime measurements, a phenomenon known as the day-night effect. Most of the studies of the day-night effect in the past decade [17, 36, 37, 38, 10, 49] have used the Mikheyev-Smirnov expression [41] to describe the effect of the earth on the solar neutrinos, introduced earlier as Eq. (1.1):

$$P_{SE} = \frac{P_S - \sin^2\theta_V + P_{2e}(1 - 2P_S)}{\cos 2\theta_V} \ . \tag{1.1}$$

Again P_{SE} is the probability that an electron neutrino originating in the sun will be measured as an electron neutrino after passing through the earth, P_S is the probability that an electron neutrino ($|\nu_e\rangle$) originating in the sun will be measured as an electron neutrino upon reaching the earth, P_{2e} is the probability that a pure $|\nu_2\rangle$ eigenstate entering the earth will be measured as an electron neutrino when it emerges, and θ_V is the vacuum mixing angle as defined in Chapter 3.

In the Refs. [10, 17] the authors have claimed that there is no day-night effect at $P_S = 1/2$. In Eq. (1.1), the properties of the earth enter only through P_{2e}, which is explicitly multiplied by $(1 - 2P_S)$. We would like to stress that the case of maximal mixing is an exception to this statement. For maximal mixing Eq. (1.1) is ill-defined, because $\cos 2\theta_V = 0$. We will now show that at maximal mixing $P_{SE} \neq 1/2$, implying a day-night effect and an often overlooked energy-dependence of the suppression of the solar neutrino flux.

Physically, the day-night effect survives because the neutrino beam reaching the earth, for all MSW solutions, is predominantly $|\nu_2\rangle$. For maximal mixing this state is half ν_e and half ν_x, but there is a definite phase relationship, $|\nu_2\rangle = (|\nu_e\rangle + |\nu_x\rangle)/\sqrt{2}$, so the density matrix is not proportional to the identity matrix. A coherent component of $|\nu_1\rangle$ is regenerated as this beam traverses the earth, leading to interference with the incident $|\nu_2\rangle$ beam. The case is rather different from the small mixing-angle case, for which Eq. (1.1) really does imply the absence of a day-night effect when $P_S = 1/2$. For a small mixing angle P_S equals $1/2$ only when conditions in the sun drive the ensemble into a density matrix proportional to the identity matrix, in which case the earth would have no effect.

4.2 Derivation of Equation (1.1)

The key assumption necessary for the derivation of Eq. (1.1) is that the neutrino beam arriving at the earth can be treated as an incoherent mixture of the two mass eigenstates $|\nu_1\rangle$ and $|\nu_2\rangle$. That is, we assume that there is no interference between the ν_1 and ν_2 components reaching the earth, or equivalently that the off-diagonal entries of the density matrix in the ν_1-ν_2 basis are negligibly small. The physical effects which cause this incoherence are discussed in Appendix 3.3. In the case of maximal mixing, the incoherence is ensured for $\Delta m^2 > 6.5 \times 10^{-9}$ eV^2 because of the energy resolution of current detectors. Other sources of incoherence include the separation of $|\nu_1\rangle$ and $|\nu_2\rangle$ wave packets in transit to the earth, the averaging over the regions in the sun where the neutrinos were produced, and the averaging over the

changing radius of the earth's orbit [24]. In Appendix 3.3 we comment on the regions of parameter space for which the assumption of incoherence is valid.

Given the assumption of incoherence, we write the fractions of $|\nu_1\rangle$ and $|\nu_2\rangle$ flux from the sun as k_1 and k_2, respectively[1]. Since there is no interference, the probability that a solar neutrino will be measured as ν_e upon reaching the surface of the earth is given by

$$\begin{aligned} P_S &= k_1 \left|\langle \nu_e|\nu_1\rangle\right|^2 + k_2 \left|\langle \nu_e|\nu_2\rangle\right|^2 \\ &= k_1 \cos^2\theta_V + k_2 \sin^2\theta_V \\ &= \cos^2\theta_V - k_2 \cos 2\theta_V \ , \end{aligned} \tag{4.1}$$

where we have used Eqs. (1.2) and the fact that $k_1 + k_2 = 1$. Similarly, the probability that a solar neutrino will be measured as ν_e after passing through the earth, when it is no longer in an incoherent superposition of the mass eigenstates, is given by

$$P_{SE} = k_1 P_{1e} + k_2 P_{2e} \ , \tag{4.2}$$

where P_{1e} (P_{2e}) is the probability that a $|\nu_1\rangle$ ($|\nu_2\rangle$) eigenstate will be measured as ν_e after traversing the earth. Finally, the unitarity of the time evolution operator implies that the state vectors of two neutrinos entering the earth as $|\nu_1\rangle$ and $|\nu_2\rangle$ must remain orthonormal as they evolve through the earth and become $|\tilde{\nu}_1\rangle$ and $|\tilde{\nu}_2\rangle$, respectively. Therefore

$$P_{1e} + P_{2e} = \left|\langle \nu_e|\tilde{\nu}_1\rangle\right|^2 + \left|\langle \nu_e|\tilde{\nu}_2\rangle\right|^2 = 1 \ . \tag{4.3}$$

Eq. (1.1) can then be obtained by using Eq. (4.1) and the above equation to eliminate P_{1e}, k_1, and k_2 from Eq. (4.2).

From the above derivation, one can see that the singularity of Eq. (1.1) at maximal mixing arises when Eq. (4.1) is solved to express k_2 in terms of P_S. For maximal

[1]For large mixing angles, $\sin^2 2\theta_V \geq 0.5$ and $5 \times 10^{-5} \leq \Delta m^2(\mathrm{eV})^2 \leq 1 \times 10^{-7}$, $k_2 \approx 1$ and $k_1 \approx 0$.

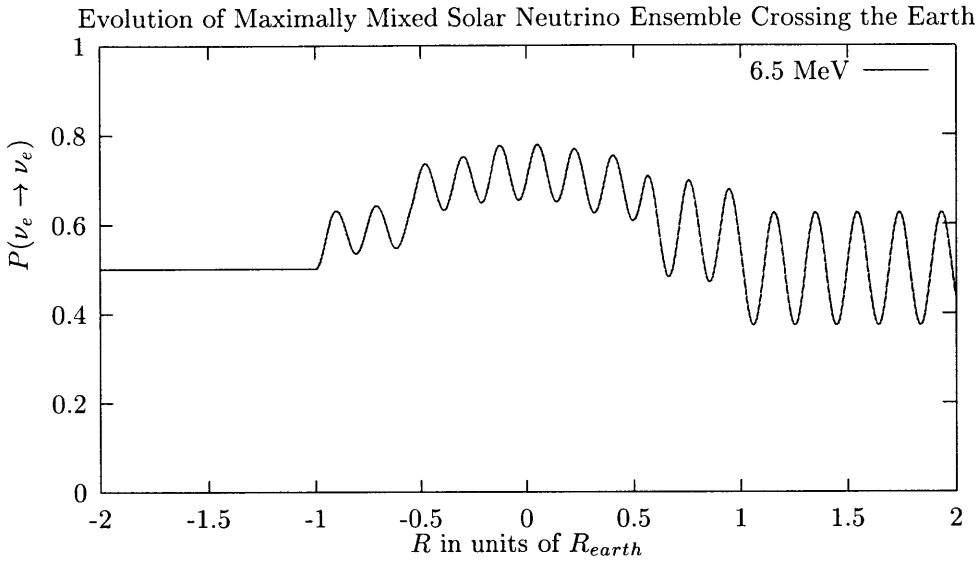

Figure 4-1: The evolution of $P_{\nu_e \to \nu_e}$ as the ensemble of neutrinos propagates across the center of the earth. The neutrinos enter the earth as an incoherent mixture of the energy eigenstates ν_1 and ν_2 which is almost completely ν_2. This plot shown is for $\Delta m^2 = 1.3 \times 10^{-5}$ eV^2 and a neutrino energy $E = 6.5$ MeV.

mixing $P_S = 1/2$ for any value of k_2, so k_2 cannot be expressed in terms of P_S. The ambiguity disappears, however, if one leaves k_2 in the answer, so Eq. (4.3) can be used to rewrite Eq. (4.2) as

$$P_{SE} = \frac{1}{2} + 2\left(k_2 - \frac{1}{2}\right)\left(P_{2e} - \frac{1}{2}\right) . \tag{4.4}$$

Thus, $P_{SE} = 1/2$ only if $k_2 = 1/2$ or $P_{2e} = 1/2$. For the MSW solutions at maximal mixing one has $k_2 \approx 1$, and there is no reason to expect $P_{2e} = 1/2$. Generically $P_{SE} \neq 1/2$ for the case of maximal mixing.

4.3 Analysis at maximal mixing

Using the evolution equations derived in Chapter 3 and the procedures described in Appendix A, we have calculated a variety of properties concerning the day-night effect for maximal mixing angle. The calculation parameters are chosen for those of the Super-Kamiokande detector.

Figure 4-1 shows the evolution of $P(\nu_e \to \nu_e)$, the probability that a solar neutrino

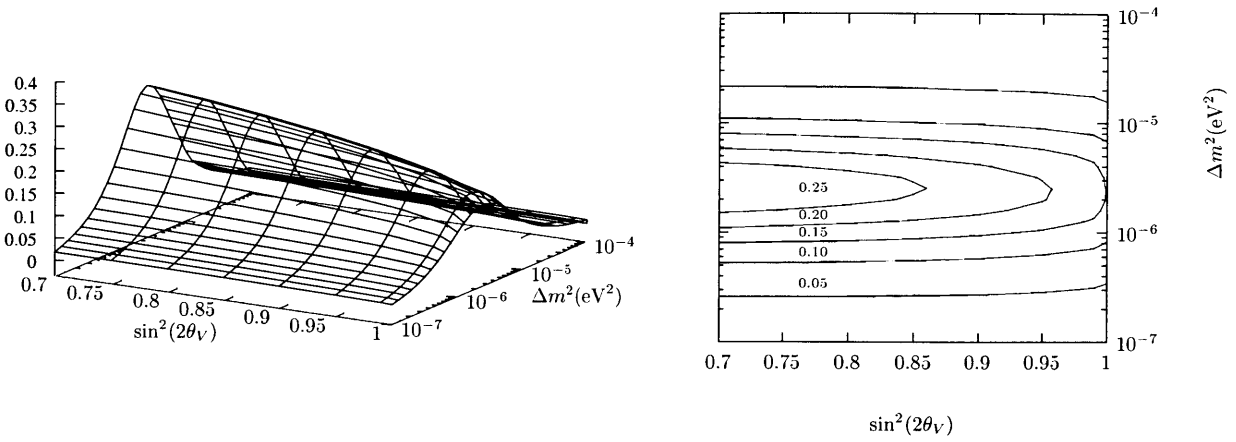

Figure 4-2: The day-night asymmetry ($A_{d-n} = (N - D)/(N + D)$) as a function of mixing parameters calculated using the density matrix. On the left is a three dimensional surface where the height of the surface is the day-night asymmetry. Notice that the exposed edge is calculated at maximal mixing and is clearly non-zero. On the right is a contour plot showing the lines of constant day-night asymmetry.

will be measured as ν_e, as the beam of neutrinos traverses a path through the center of the earth. Notice that after traversing the earth the ensemble of neutrinos is no longer in a steady state, but instead $P(\nu_e \to \nu_e)$ continues to oscillate in the vacuum. From the perspective of the mass eigenstates, the neutrinos under consideration arrive at the earth roughly in a $|\nu_2\rangle$ state. Upon reaching the earth, the step-function-like changes in the electron density profile (see Fig. A-1) cause non-adiabatic evolution, regenerating the $|\nu_1\rangle$ state and leading to interference effects. In the regions of parameter space where the day-night effect is maximal because the oscillation length of these interference terms coincides with the length of the slabs of near constant density composing the earth, the resulting buildup of ν_e flux has been called oscillation length resonance [44, 45, 2].

In Fig. 4-2 we present a contour plot calculated from the density matrix that exemplifies the non-zero nature of the day-night effect at maximal mixing. On the left is a three-dimensional surface where the height of the surface is the day-night asymmetry. Notice that the exposed edge is calculated at maximal mixing and is clearly non-zero. On the right is a contour plot showing the lines of constant day-night asymmetry, a plot which is identical to those produced in other references.

4.4 Induced energy dependence

We now explain how the inclusion of the day-night effect at maximal mixing resolves a certain confusion that has arisen in the past because of its neglect. As a result of the non-zero day-night effect, there exists an energy dependence at maximal mixing, as can be seen in Fig. 4-3. If one assumes that the flux suppression at maximal mixing has no energy dependence, as was done in Ref. [30], then there is an apparent discrepancy between two sections of Ref. [12]. Sec. IV-D excludes the possibility of energy-independent oscillation into active (as opposed to sterile) neutrinos at the 99.8% confidence level, while Fig. 2 shows some regions of the maximal-mixing-angle parameter space not excluded at the 99% confidence level (we have reproduced Fig. 2 of Ref. [12] as Fig. 3-1 in this thesis). Ref. [30] has tried to resolve this discrepancy without including the day-night effect, concluding that maximal mixing is excluded at the 99.6% confidence level. The actual resolution to this apparent discrepancy is that Fig. 2 of Ref. [12] includes the energy dependence induced by the day-night effect at maximal mixing, while Sec. IV-D discusses the case of energy-independent flux suppression and does not apply to maximal mixing. The correct conclusion is that of Fig. 2, which shows that maximal mixing is not excluded at the 99% confidence level.

Whether or not the day-night effect is included, maximal mixing is not a very good fit to the experimental data from the three neutrino experiments (chlorine, gallium, and water) [12]. However, maximal mixing does fit well if the chlorine data is excluded on the suspicion of some systematic error [46]. Ref. [18] has argued that if the ^8B flux is about 17% lower than the standard solar model (BP98) [8], then a bi-maximal mixing scenario becomes a tenable solution to the solar neutrino problem. The MSW mechanism described here is applicable for $\Delta m^2 > 6.5 \times 10^{-9}$ eV^2. In the bi-maximal mixing scenario that we consider the upper bound on Δm^2 is set by the CHOOZ data constraining $\Delta m^2 \leq 0.9 \times 10^{-3}$ eV^2 [47].

When detailed studies of the day-night effect are completed, the energy (and zenith angle) dependence will be valuable additional information. To the best of our knowledge, the Super-Kamiokande Collaboration has not published their day-night

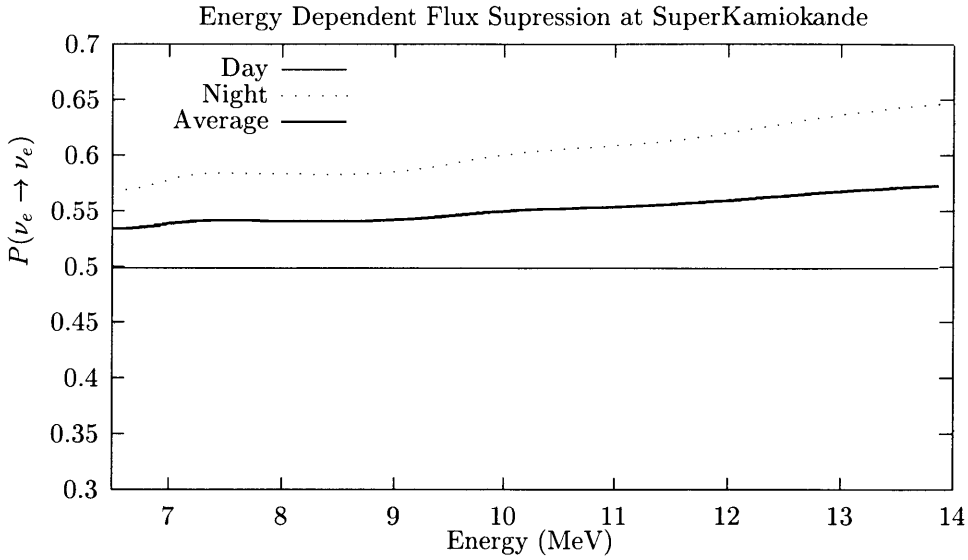

Figure 4-3: The predicted flux suppression as a function of energy. Notice that the predicted overall flux suppression is not 1/2, due to day-night effects, even though the mixing angle is maximal. The plot is for $\Delta m^2 = 1.0 \times 10^{-5}$ eV^2 which is near the border of the region excluded by the small day-night effect (A_{d-n}) measured at Super-Kamiokande.

asymmetry as a function of recoil electron energy. Past studies of the day-night effect have noted the energy dependence of the day-night asymmetry [38, 10]. While for small mixing angles $|A_{d-n}| < 0.02$ without a clear energy dependence [10], for large mixing angles the A_{d-n} energy dependence can be significant and informative. Fig. 4-4 shows the theoretical predictions of the day-night asymmetry in the electron recoil spectrum at Super-Kamiokande for two cases of maximal mixing: $\Delta m^2 = 2\times10^{-5}$ eV^2 and $\Delta m^2 = 3 \times 10^{-7}$ eV^2. Note that the two curves have opposite slopes.

The approximate shape of the graph of A_{d-n} vs. recoil electron energy can be understood from Fig. 4-2, using the fact that Fig. 4-2 is dominated by the peak of the ^8B neutrino spectrum at about 6.5 MeV. It is shown in Appendix 3.2 that the neutrino evolution equations (Eqs. (3.7)-(3.10)) depend on Δm^2 and the neutrino energy (or momentum) E only through the combination $\Delta m^2/E$. Thus, Fig. 4-2 shows that for any value of $\sin^2 2\theta_V$, A_{d-n} has a maximum at $\Delta m^2/E \approx 2.5 \times 10^{-6}$ eV^2/(6.5 MeV).

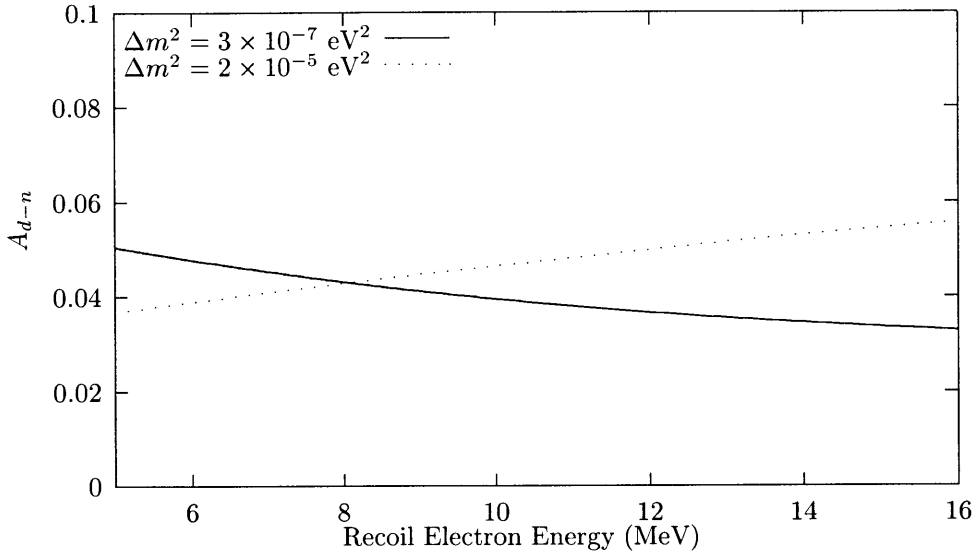

Figure 4-4: The day-night asymmetry ($A_{d-n} = (N - D)/(N + D)$) as a function of recoil electron energy at Super-Kamiokande. Both plots are at maximal mixing angle, with Δm^2 at the upper and lower borders of the region disfavored by the smallness of the day-night effect observed at Super-Kamiokande. The rising line is for $\Delta m^2 = 2 \times 10^{-5}$ eV^2, and the descending line is for $\Delta m^2 = 3 \times 10^{-7}$ eV^2.

When E is varied at fixed Δm^2, A_{d-n} will have a peak at

$$E \approx \frac{\Delta m^2}{2.5 \times 10^{-6}\ \text{eV}^2} \times 6.5\ \text{MeV} \ . \tag{4.5}$$

So for $\Delta m^2 = 2 \times 10^{-5}$ eV^2 the peak lies far to the right of the scale in Fig. 4-4, so the curve slopes upward. For $\Delta m^2 = 3 \times 10^{-7}$ eV^2 the peak lies far to the left, and the curve slopes downward.

Fig. 4-2 shows that the peak in the graph of A_{d-n} vs. Δm^2 is higher at large mixing angles ($\sin^2 2\theta_V \approx 0.7$) than it is at maximal mixing, so the same will be true for the energy dependence of the day-night effect. For $\sin^2 2\theta_V = 0.63$ and $\Delta m^2 = 1.3 \times 10^{-5}$ eV^2, for example, the slope of the graph of A_{d-n} vs. recoil electron energy is about twice the magnitude of the slopes shown in Fig. 4-4. Thus, the day-night asymmetry as a function of recoil electron energy could be a strong indicator of Δm^2 if the solar neutrinos have a large or maximal mixing angle in the MSW range of parameters.

Chapter 5

Conclusions

In this thesis we have reviewed the solar neutrino problem, and we have derived the MSW solution to the solar neutrino problem. We have also derived the Eq. (1.1) for calculations of the day-night effect. We have pointed out that Refs. [10, 17] incorrectly assume that that $P_S = 1/2$ always implies $P_{SE} = 1/2$. We have also shown that neutrinos with a maximal mixing angle can have a day-night effect and that they do not always result in a uniform energy-independent flux suppression of 1/2. Because the issues that we have attempted to clarify concern mainly the words that have been used to describe correct equations (which were generally used numerically), there are no changes to most constraints presented in other references. The only corrections apply to fits of energy-independent suppressions; that is, in contradiction with the assumptions of Ref. [30], the fits do not apply to the exclusion of some regions of maximally mixed neutrinos. Finally, we have noted that the energy dependence of the day-night effect can be a strong discriminator between various solutions of the solar neutrino problem.

Appendix A

Calculation Methodology for the Day-Night Effect

First we calculated P_S using Eq. (3.36) for the spectrum of $\Delta m^2/p$ at various mixing angles. For a given $\Delta m^2/p$ we averaged P_S over the regions of ^8B neutrino production in the sun, provided by Ref. [6]. Using P_S to describe the neutrinos that arrive at the earth, we then performed the evolution through the earth with the density matrix equations of motion. The initial conditions for the density matrix are given by

$$\rho_{ee} = P_S, \tag{A.1}$$

and

$$\rho_{xe} = -\frac{1}{2}(2P_S - 1)\tan 2\theta_V. \tag{A.2}$$

At maximal mixing we assume that $\rho_{xe} = -\frac{1}{2}\cos\Big(2\theta_M(t_0)\Big)\sin 2\theta_V \approx \frac{1}{2}$ which is the adiabatic result. This assumption is justified because in the regions of parameter space under consideration near maximal mixing, $P_{\text{jump}} \approx 0$. It follows that in these same regions of parameter space the evolution remains adiabatic in the limit where $\theta_V = \pi/4$. We use the earth density profile given in the Preliminary Reference Earth Model (PREM) [25] (see Fig A-1). To convert from the mass density to electron number density we use the charge to nucleon ratio $Z/A = 0.497$ for the mantle

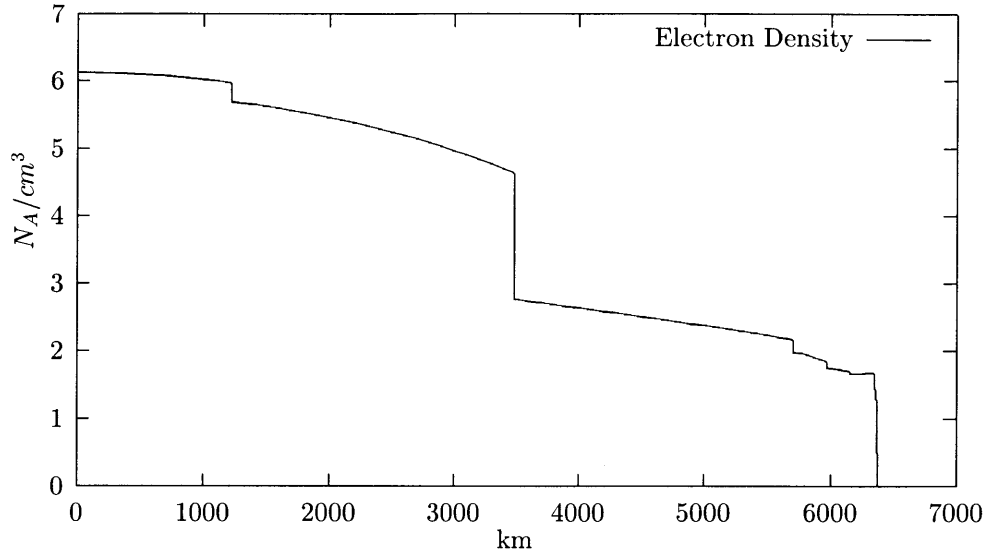

Figure A-1: The Preliminary Reference Earth Model (PREM) electron density (N_e) profile of the earth. N_e is shown in units of Avogadro's number of electrons per cm^3.

and $Z/A = 0.467$ for the core. The numerical calculations were performed using a fourth order Runge-Kutta integration programmed in C++. We propagated the neutrinos through the earth for 90 zenith angles, α, evenly spaced between 90 and 180 degrees. We calculate the anticipated electron flux as a function of zenith angle and energy, denoted $P_{SE}(\alpha, E_\nu)$. The calculation parameters are chosen for those of the Super-Kamiokande detector. The normalized ^8B neutrino spectrum, $\Phi(E_\nu)$, and solar electron densities, N_e, are also obtained from data-files provided by Ref. [6]. Effective neutrino cross sections are available which take into account the electron recoil cross section with radiative corrections, the energy resolution, and the trigger efficiency [11, 6]. We used these more accurate cross sections for the overall day-night effect plotted in Fig. 4-2. Because these effective cross sections already include the integration over detected electron recoil energy, to calculate the recoil electron spectrum we used the differential neutrino-electron scattering cross sections given in Ref. [4]. Using these data files and numerical results the cross section for the scattering of solar neutrinos of energy E_ν with electrons to produce a recoil electron of energy T' at the zenith angle α is given by

$$\frac{d\sigma_{\nu_{\rm solar}}}{dT'}(T', E_\nu, \alpha) = P_{SE}(\alpha, E_\nu)\frac{d\sigma_{\nu_e}}{dT'}(T', E_\nu) + [1 - P_{SE}(\alpha, E_\nu)]\frac{d\sigma_{\nu_\mu}}{dT'}(T', E_\nu). \quad \text{(A.3)}$$

Since muon and tau neutrinos have the same neutral current interactions, we can use the ν_μ cross section for the ν_x. The analysis of the recoil electron spectra is explained in Refs. [11]. The actual flux at recoil energy, T, is

$$g(\alpha, T) = \int_0^\infty dE_\nu \; \Phi(E_\nu) \int_0^{T'_{\max}} dT' \; R(T, T') \; \frac{d\sigma_{\nu_{\text{solar}}}}{dT'}(T', E_\nu, \alpha) \tag{A.4}$$

where the energy resolution of the detector is incorporated through

$$R(T, T') = \frac{1}{\Delta_{T'}\sqrt{2\pi}} \exp\left(\frac{-(T' - T)^2}{2\Delta_{T'}^2}\right). \tag{A.5}$$

The energy resolution, $\Delta_{T'}$, around the true electron energy T' for Super-Kamiokande is given by

$$\Delta_{T'} = (1.6 \text{ MeV}) \sqrt{T'/(10 \text{ MeV})}. \tag{A.6}$$

To calculate the average day-night effect over one year, we weight the flux by the zenith angle exposure function $Y(\alpha)$ explained in Appendix B. The daytime measured flux at a given measured electron recoil energy, T, is given by

$$D(T) = \int_0^{90} d\alpha \; g(\alpha, T) Y(\alpha), \tag{A.7}$$

and for nighttime is

$$N(T) = \int_{90}^{180} d\alpha \; g(\alpha, T) Y(\alpha). \tag{A.8}$$

The day-night asymmetry as a function of recoil electron energy plotted in Fig. 4-4 is given by

$$A_{d-n}(T) = \frac{N(T) - D(T)}{N(T) + D(T)}. \tag{A.9}$$

The final day-night asymmetry plotted in Fig. 4-2 is given by

$$A_{d-n} = \frac{\int_{5 \text{ MeV}}^\infty dT \; \Big(N(T) - D(T)\Big)}{\int_{5 \text{ MeV}}^\infty dT \; \Big(N(T) + D(T)\Big)} \tag{A.10}$$

where 5 MeV is the minimum energy detected at Super-Kamiokande. Verification of the accuracy of the computer code has been accomplished with the help of [35], and

by comparing our simulations to plots and data available in the literature.

Appendix B

The Zenith Distribution Function

The zenith angle distribution function gives the fraction of the time that the sun is at a given zenith angle. The function is calculated by numerically simulating the orbit of the earth around the sun. We begin by writing the vector towards the zenith of the detector in coordinates for which the earth's orbit lies in the x-y plane:

$$\vec{r}_z = \begin{pmatrix} 1 & 0 & 0 \\ 0 & \cos\delta & -\sin\delta \\ 0 & \sin\delta & \cos\delta \end{pmatrix} \begin{pmatrix} \sin(90^\circ - L)\cos\phi \\ \sin(90^\circ - L)\sin\phi \\ \cos(90^\circ - L) \end{pmatrix} \tag{B.1}$$

where the north latitude is given by L, ϕ gives the time of day in radians, and $\delta = 23.439^\circ$ is the earth's declination [1]. Because we are averaging over a one year time period we can arbitrarily choose the initial time of year, and the initial time of day. The vector pointing from the earth towards the sun is

$$\vec{r}_s = \begin{pmatrix} \cos D \\ \sin D \\ 0 \end{pmatrix} \tag{B.2}$$

where D is the day of the year in radians. From here we can find the local zenith angle from the dot product $\vec{r}_s \cdot \vec{r}_z = \cos\alpha$. To numerically calculate the zenith function distribution we divided α into 360 bins evenly spaced between 0 and π. Now we run $0 \leq D \leq 2\pi$ and $0 \leq \phi \leq 2\pi$ over 1000 steps in D and 1000 steps in ϕ and

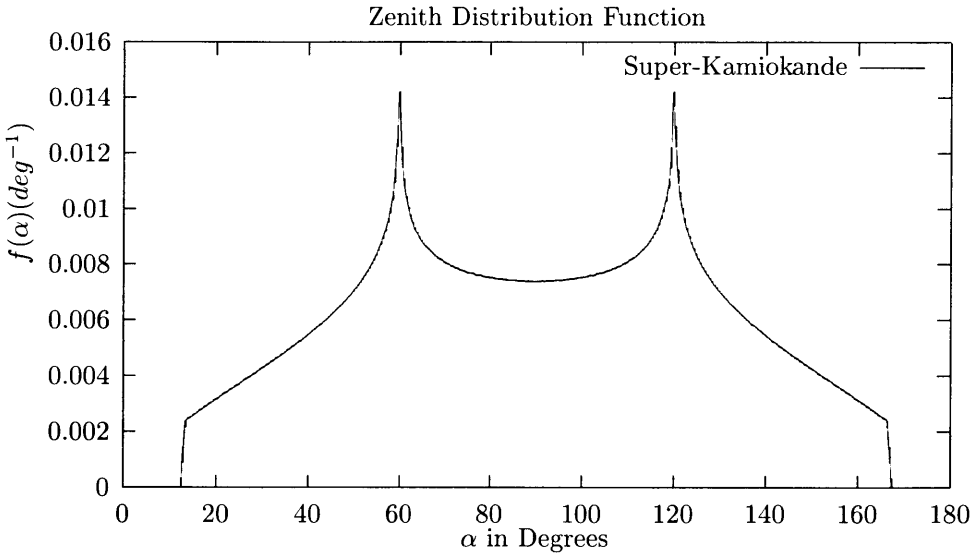

Figure B-1: The zenith distribution function at Super-Kamiokande.

count how much relative time α spends over each bin. We generate the zenith angle distribution function for Super-Kamiokande which sits in Gifu Prefecture, Japan at 36.43° north latitude [49]. This produces the undistorted zenith function distribution seen in Fig. B-1. One can also obtain this function as a data file from [6] which includes small corrections for the eccentricity of the earth's orbit and the wobble of the earth's declination. To maximize accuracy we performed our calculations using this data file.

Bibliography

[1] *The Astronomical Almanac.* US Government Printing Office, 1996.

[2] E. Akhmedov. Remarks on parametric resonance of neutrino oscillations in the earth. 1999. hep-ph/9903302.

[3] J. N. Bahcall. Solar neutrinos. I. theoretical. *Phys. Rev. Lett.*, 12:300, 1964.

[4] J. N. Bahcall. *Neutrino Astrophysics.* Cambridge University Press, 1989.

[5] J. N. Bahcall. An introduction to solar neutrino research. 1997. hep-ph/9711358.

[6] J. N. Bahcall, 1998. http://www.sns.ias.edu/$\tilde{\text{j}}$nb/.

[7] J. N. Bahcall and et. al. Proposed solar-neutrino experiment using ^{71}Ga. *Phys. Rev. Lett.*, 13:332, 1964.

[8] J. N. Bahcall, Sarbani Basu, and M.H. Pinsonneault. How uncertain are solar neutrino predictions? *Phys. Lett. B*, 433:1, 1998.

[9] J. N. Bahcall, W. A. Fouler, I. Iben, and R. .L. Sears. Solar neutrino flux. *Ap. J.*, 137:L344, 1963.

[10] J. N. Bahcall and P. I. Krastev. Does the sun appear brighter at night in neutrinos? *Phys. Rev. C*, 56:2839, 1997. hep-ph/9706239.

[11] J. N. Bahcall, P. I. Krastev, and E. Lisi. Neutrino oscillations and moments of electron spectra. *Phys. Rev. C*, 55:494, 1997. nucl-ex/9610010.

[12] J. N. Bahcall, P. I. Krastev, and A. Yu. Smirnov. Where do we stand with solar neutrino oscillations? *Phys. Rev. D*, 58:096016, 1998. hep-ph/9807216.

[13] J. N. Bahcall and Plamen Krastev. Do hep neutrinos affect the solar neutrino energy spectrum? *Phys. Lett. B*, 436:243, 1998. hep-ph/9807525.

[14] A. B. Balantekin. Exact solutions for matter-enhanced neutrino oscillations. *Phys. Rev. D*, 58:013001, 1998. hep-ph/9712304.

[15] A. B. Balantekin and J. F. Beacom. Semiclassical treatment of matter-enhanced neutrino oscillations for an arbitrary density profile. *Phys. Rev. D*, 54:6323, 1996. hep-ph/9606353.

[16] A. J. Baltz and J. Weneser. Effect of transmission through the earth on neutrino oscillations. *Phys. Rev. D*, 35:3364, 1987.

[17] A. J. Baltz and J. Weneser. Implication of gallium results on the possibility of observing day-night matter oscillations at SNO Super-Kamiokande and BOREXINO. *Phys. Rev. D*, 50:5971, 1994.

[18] Anthony J. Baltz, Alfred Scharff Goldhaber, and Maurice Goldhaber. The solar neutrino puzzle; an oscillation solution with maximal neutrino mixing. *Phys. Rev. Lett.*, 81:5730, 1998. hep-ph/9806540.

[19] V. Barger, S. Pakvasa, T.J. Weiler, and K. Whisnant. Bi-maximal mixing of three neutrinos. *Phys. Lett. B*, 437:107, 1998. hep-ph/9806387.

[20] V. Barger and K. Whisnant. Seasonal and energy dependence of solar neutrino vacuum oscillations. 1999. hep-ph/9903262.

[21] Eric D. Carlson. Terrestrially enhanced neutrino oscillations. *Phys. Rev. D*, 34:1454, 1986.

[22] S. Davidson and S.F. King. Bi-maximal neutrino mixing in the MSSM with a single right-handed neutrino. *Phys. Lett. B*, 445:191, 1999. hep-ph/9808296.

[23] Raymond Davis, Dos Harmer, and Kenneth Hoffman. Search for neutrinos from the sun. *Phys. Rev Lett.*, 20:1205, 1968.

[24] Amol Dighe, Q. Liu, and A. Yu. Smirnov. Coherence and the day-night asymmetry in the solar neutrino flux. 1999. hep-ph/9903329.

[25] Adam M. Dziewonski and Don L. Anderson. Preliminary reference earth model. *Physics of the Earth and Planetary Interiors*, 1981.

[26] Peter V. Foukal. *Solar Astrophysics.* John Wiley and Sons, Inc., 1990.

[27] H. Fritzsch and Z. Z. Xing. Lepton mass hierarchy and neutrino oscillations. *Phys. Lett. B*, 372:265, 1996.

[28] H. Fritzsch and Z. Z. Xing. Large leptonic flavor mixing and the mass spectrum of leptons. *Phys. Lett. B*, 440:313, 1998. hep-ph/9808272.

[29] GALLEX Collaboration. GALLEX results from the first 30 solar neutrino runs. *Phys Lett. B*, 327:377, 1994.

[30] C. Giunti. Is bi-maximal mixing compatible with the large angle msw solution of the solar neutrino problem? *Phys. Rev. D*, 59:077301, 1999. hep-ph/9810272.

[31] J. N. Abdurashitov et. al. Results for SAGE. *Phys. Lett. B*, 328:234, 1994.

[32] K. S. Hirata, et. al. Results from one thousand days of real-time, directional solar-neutrino data. *Phys. Rev. Lett.*, 65:1297, 1990.

[33] Sin Kyu Kang and C. S. Kim. Bi-maximal lepton flavor mixing matrix and neutrino oscillation. *Phys. Rev. D*, 59:091302, 1999. hep-ph/9811379.

[34] C. W. Kim and A. Pevsner. *Neutrinos in Physics and Astrophysics.* Harwood Academic Publishers, 1993.

[35] P. I. Krastev, 1999. Private Communications.

[36] Eligio Lisi and Daniele Montanino. Earth regeneration effect in solar neutrino oscillations: an analytic approach. *Phys. Rev. D*, 56:1792, 1997. hep-ph/9702343.

[37] Q. Y. Liu, M. Maris, and S. T. Petcov. A study of the day night effect for the Super-Kamiokande I: Time averaged solar neutrino probability. *Phys. Rev. D*, 56:5991, 1997.

[38] M. Maris and S.T. Petcov. A study of the day-night effect for the Super-Kamiokande detector: II. electron spectrum deformations and day-night asymmetries. *Phys. Rev. D*, 56:7444, 1997. hep-ph/9705392.

[39] S. P. Mikheyev and A. Yu. Smirnov. *Soviet Journal of Nuclear Physics*, 42:913, 1985.

[40] S. P. Mikheyev and A. Yu. Smirnov. *Nuovo Cimento C*, 9:17, 1986.

[41] S. P. Mikheyev and A. Yu. Smirnov. Resonance oscillations of neutrinos in matter. *Soviet Physics – USPEKHI*, 30:759, 1987.

[42] Yasunori Nomura and T. Yanagida. Bi-maximal neutrino mixing in SO(10) GUT. *Phys. Rev. D*, 59:017303, 1999. hep-ph/9807325.

[43] Stephen Parke. Nonadiabatic level crossing in resonant neutrino oscillations. *Phys. Rev. Lett.*, 57:1275, 1986.

[44] Serguey Petcov. Diffractive-like (or parametric-resonance-like?) enhancement of the earth (day-night) effect for solar neutrinos crossing the earth core. *Phys. Lett. B*, 434:321, 1998. hep-ph/9805262.

[45] Serguey Petcov. The oscillation length resonance in the transition of solar and atmospheric neutrinos crossing the earth core. 1998. hep-ph/9811205.

[46] R. Barbieri et al. Oscillations of solar and atmospheric neutrinos. *JHEP*, 12:017, 1998. hep-ph/9807235.

[47] The CHOOZ Collaboration (M. Apollonio et al.). Initial results from the CHOOZ long baseline reactor neutrino oscillation experiment. *Phys. Lett. B*, 420:397, 1998. hep-ex/9711002.

[48] L Wolfenstein. Neutrino oscillations in matter. *Phys. Rev. D*, 17:2369, 1978.

[49] Y. Fukuda and The Super-Kamiokande Collaboration. Constraints on neutrino oscillation parameters from the measurement of day-night solar neutrino fluxes at Super-Kamiokande. *Phys. Rev. Lett.*, 82:1810, 1999. hep-ex/9812009.